Spin transport across the interface in ferromagnetic/nonmagnetic systems

C. Swindells,[1] A. T. Hindmarch,[1] A. J. Gallant,[2] and D. Atkinson[1,*]
[1]*Department of Physics, Durham University, Durham DH1 3LE, United Kingdom*
[2]*Department of Engineering, Durham University, Durham DH1 3LE, United Kingdom*

(Received 19 October 2018; published 5 February 2019)

Understanding interfacial spin transport is key to developing magnetoelectonic devices, however, the exact nature of the parameters involved is unclear. Here, we report a detailed ferromagnetic resonance-based spin-transport analysis on a variety of structures of both ferromagnetic (Co, CoFeB) and heavy metal layers (Pt, Ru) in order to fully quantify the interfacial spin-transport parameters. Enhanced spin-mixing conductance is observed for more closely matched ferromagnet and heavy metal crystal structures, and, significantly, the inclusion of a thickness-dependent spin-diffusion length gives a bulk value of 9.4 ± 0.7 nm for Pt, resolving reported discrepancies.

DOI: 10.1103/PhysRevB.99.064406

I. INTRODUCTION

The transport of spin information across interfaces in ferromagnetic (FM)/nonmagnetic (NM) multilayer systems is fundamental to spintronic physics and the resulting applications. Spin current, generated via the spin Hall effect [1], flows from a NM heavy metal into a FM layer with the flow of charge current in the NM layer. Spin current also flows from a FM layer into a NM layer as a result of magnetization precession within the FM layer, through a process termed spin pumping that enhances the precessional damping.

Spin transport across FM/NM interfaces is determined by a combination of factors associated with the materials involved and details of the interface, which have become embodied within the effective spin-mixing conductance $g_{\mathrm{eff}}^{\uparrow\downarrow}$ [2–4], higher values of which are associated with enhanced damping. The spin-mixing conductance depends upon the thickness and saturation magnetization of the FM layer and, more significantly, it also depends on the spin-diffusion length of the NM layer and spin-flip scattering associated with the interfacial structure, which has been termed spin-memory loss [5,6] or the spin-flip probability at the interface [7,8].

These latter parameters remain the subject of debate, with the reported values seemingly affected by the different experimental methods and analyses. In particular, values for the spin-diffusion length of the NM layer are inconsistent, while the role of the interface structure and its influence on the effective spin-diffusion length are not clear. The transport properties of such systems have been probed with several techniques, including magnetoresistance [5,9,10], magneto-optics [11], spin Hall angle [12–14], ferromagnetic resonance (FMR) [15–20], and combinations of these techniques [6,21–23]. A range of values for the spin-diffusion length λ_{sf} have been reported for Pt at room temperature from 1.2 nm up to 11 nm [11,13] from these different methods, with FMR measurements giving lower values for λ_{sf} than spin Hall measurements [13,18,24,25].

The physical basis of the interfacial contribution is ascribed to additional spin-flip scattering associated with an effective interface thickness due to disorder [6], however, it was shown theoretically for an atomically flat FM/heavy metal interface that *d-d* hybridization enhances the damping [26], which effectively increases $g_{\mathrm{eff}}^{\uparrow\downarrow}$. Furthermore, the influence on spin pumping and the spin-mixing conductance of crystallographic structuring at the interface has recently been demonstrated [27–29]. Experiments on the relation between the thickness dependence of very thin NM layers (<2 nm) on damping highlight the important role of the interfacial structure [30] and also suggest that proximity-induced magnetization may play a role [15,31].

Despite the range of systems studied in the literature, the factors affecting spin transport across FM/NM boundaries remain the subject of debate. The contributions to $g_{\mathrm{eff}}^{\uparrow\downarrow}$ related to interfacial structure, spin-diffusion length, and spin Hall angle are not clearly defined. Spin-mixing conductance is often quoted for a single NM thickness, which can lead to $g_{\mathrm{eff}}^{\uparrow\downarrow}$ behaving as a catch-all term that critically affects the determination of the spin-diffusion length.

This paper details an FMR-based study of spin-mixing conductance to determine the role of the interface and obtain reliable values for the spin-diffusion length in FM/NM systems. The contributions of interfacial effects and the spin-diffusion length to $g_{\mathrm{eff}}^{\uparrow\downarrow}$ were studied with an amorphous (CoFeB/Pt) and two different crystalline (Co/Pt and Co/Ru) interfacial textures as a function of the thickness of the NM and FM layers.

Transition metals such as Ru and Pt are particularly useful for enhancing damping in FM/NM systems via spin pumping mechanisms [17,32], for control of perpendicular magnetic anisotropy (PMA) [33,34], and for enhancing spin-orbit torques when used in combination [35]. For these materials it is expected that spin relaxation follows the mechanisms outlined by the Elliot-Yafet (EY) theory [36–38]. The EY mechanism involves a probabilistic spin-flip scattering at each momentum scattering event, with the spin relaxation time τ_s and λ_{sf} proportional to the momentum scattering time and

*del.atkinson@durham.ac.uk

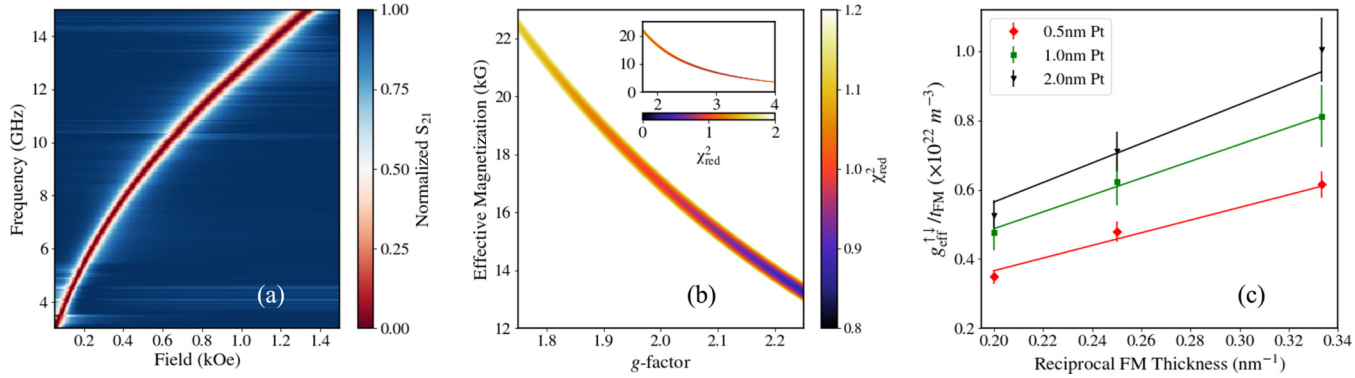

FIG. 1. (a) A broadband frequency and field FMR spectra. (b) Reduced χ^2 plot of the fit for a Kittel curve for various M_{eff} and g values. Note that the there exists a range for which both variables produce very similar best fits with χ^2. The inset is χ^2 over a larger range of variables. (c) Effective spin-mixing conductance for each NM thickness, extracted from the gradient of the line, without requiring specific fitting for g or α, as in Eq. (4).

the mean free path, τ and l. This contrasts with D'yakonov-Perel spin relaxation [39], which involves a gradual dephasing of spins.

Recently, Sagasta *et al.* showed a dependence of λ_{sf} on the resistivity ρ for thin-film Pt [40] and building on this Nguyen *et al.* showed the product $\lambda_{\text{sf}}\rho$ is a constant for a given NM layer [41]. Considering this dependence of λ_{sf} on ρ, the work here presents the results of a study on the *thickness* dependence of the NM layer, as a route to determine reliable values of λ_{sf} using FMR.

II. METHODS, ANALYSIS, AND EXPERIMENTAL DETAILS

FMR measurements were carried out using a vector network analyzer (VNA) at room temperature, over both a wide frequency and magnetic field range [42]. Figure 1(a) shows an example of the frequency and magnetic field relationship of the ferromagnetic resonance measured from the S_{21} parameter. The resonant linewidth in magnetic field ΔH as a function of frequency f allows the intrinsic and extrinsic contributions to damping to be extracted via

$$\Delta H = \Delta H_0 + \frac{4\pi\alpha}{\gamma} f, \tag{1}$$

where ΔH_0 is the extrinsic damping related to defects [30], α the intrinsic Gilbert damping parameter, and γ the gyromagnetic ratio. The gyromagnetic ratio can be expressed in terms of the spectroscopic g-factor using $\gamma = g\mu_{\text{B}}/\hbar$. This relation also assumes no periodic defects in the sample [43,44]. The intrinsic damping parameter α can be described by a combination of bulk, α_0, and interface, $\Delta\alpha$, terms, with the latter given by

$$\Delta\alpha = \alpha - \alpha_0 = \frac{\gamma\hbar}{4\pi M_{\text{s}} t_{\text{FM}}} g^{\uparrow\downarrow}_{\text{eff}}, \tag{2}$$

which is dependent on the effective spin-mixing conductance. The resonant condition for in-plane FMR of a thin film is given by the Kittel formula [45],

$$f = \frac{\gamma}{2\pi}\sqrt{H_{\text{res}}(H_{\text{res}} + 4\pi M_{\text{eff}})}, \tag{3}$$

with H_{res} the magnetic field at resonance, and the effective magnetization M_{eff} that takes into account any interfacial anisotropy terms. The spectroscopic g-factor (via γ) in Eq. (3) can complicate the fitting of resonance curves. The g-factor is given by the ratio of the orbital, μ_{L}, to the spin, μ_{S}, magnetic moments commonly given as $g = 2(1 \pm \mu_{\text{L}}/\mu_{\text{S}})$ [46]. In bulk systems the orbital term is quenched by the crystal field, however, at the interfaces, symmetry is broken, leading to an enhancement in μ_{L}. For analysis of single-axis FMR measurements, both the g-factor and M_{eff} fitting parameters are correlated. Figure 1(b) shows the range of these parameters that gives comparable fits with similar reduced chi squared χ^2_{red} for the same data. There is a further complication regarding the observed angular dependence of ΔH that has been attributed to a g-tensor [44,47] or more recently to anisotropic Gilbert damping [48]. In addition, both the g-factor [49] and M_{eff} are influenced by the thickness of surrounding layers [33,34]. Here, the focus is on spin transport across the interface, so rearranging Eq. (2) gives

$$\frac{g^{\uparrow\downarrow}_{\text{eff}}}{t_{\text{FM}}} = \frac{M_{\text{s}}}{\hbar}\left(\frac{4\pi\,\Delta\alpha}{\gamma}\right), \tag{4}$$

which allows direct extraction of $g^{\uparrow\downarrow}_{\text{eff}}$ using the second term of Eq. (1), that depends only on the ratio of α and the g-factor. Figure 1(c) shows examples, based on Eq. (4), that directly give $g^{\uparrow\downarrow}_{\text{eff}}$ from the gradient, and the bulk term from the intercept of the best fits to the data [27].

The measurement of $g^{\uparrow\downarrow}_{\text{eff}}$ as a function of NM thickness allows the interfacial transport parameters to be extracted. Following Tserkovnyak *et al.* [8], interfacial damping depends on the NM thickness according to

$$\Delta\alpha = \frac{\alpha^{\infty}_{\text{sp}}\sqrt{\epsilon}}{\sqrt{\epsilon} + \coth\left(\frac{t_{\text{NM}}}{\lambda_{\text{sf}}}\right)}, \tag{5}$$

where ϵ is the spin-flip probability in the NM layer, required to be $\geqslant 10^{-3}$ in its derivation [8]. The linear relationship between $g^{\uparrow\downarrow}_{\text{eff}}$ and $\Delta\alpha$ means they follow the same dependence on NM thickness, so

$$g^{\uparrow\downarrow}(t_{\text{NM}}) = \frac{g^{\uparrow\downarrow}_{\infty}\sqrt{\epsilon}}{\sqrt{\epsilon} + \coth\left(\frac{t_{\text{NM}}}{\lambda_{\text{sf}}}\right)}, \tag{6}$$

with a bulk term $g^{\uparrow\downarrow}_{\infty}$ at $t_{\text{NM}} \gg \lambda_{\text{sf}}$. The value of $g^{\uparrow\downarrow}_{\text{eff}}$ is often only determined by Eq. (6), and therefore only is valid at a

single NM thickness, however, using Eq. (5) allows for $g_{\text{eff}}^{\uparrow\downarrow}$ to be fully described. The spin-diffusion length is usually assumed to be constant, however, as discussed earlier, it has been shown to be proportional to the conductivity of the NM layer and therefore is expected to change for very thin films, particularly incomplete layers. Following the model of Nguyen *et al.* [41], the value of the product $\lambda_{\text{sf}}\rho$ is taken as a constant. Here, using this constant and assuming an empirical exponential dependence of ρ on the NM thickness [50], a relationship for the thickness dependence of $\lambda_{\text{sf}}(t)$ was obtained,

$$\lambda_{\text{sf}}(t) = \frac{\lambda_\infty \rho_\infty}{\rho_\infty + \frac{\lambda_\infty \rho_\infty}{\lambda_0} e^{-t/\lambda_\infty}}, \tag{7}$$

where the bulk NM resistivity and spin-diffusion length are given by ρ_∞ and λ_∞, respectively. This empirical thickness dependence of the resistivity is a stronger function of thickness than the Fuchs-Sondheimer [51,52] or Mayadas-Shatzkes models [53] and is supported by experimental thin-film studies [50,54]. Here, λ_0 (or alternatively ρ_0 [50]) is a phenomenological scaling parameter, such that the spin-diffusion length tends to zero in the limiting case of NM thickness tending to zero. The spin-flip probability ϵ is given by the ratio of the elastic scattering length to the spin-diffusion length, $l_e^2/3\lambda_{\text{sf}}^2$, which are both linearly proportional to the conductivity, therefore ϵ will not vary with NM thickness. The same $\lambda_{\text{sf}}(t)$ relation with thickness can also be derived from the spin drift equations [8] by varying the boundary conditions [55]. For the case of a FM/NM1(t)/NM2 system, the behavior of $g_\infty^{\uparrow\downarrow}$ and $\Delta\alpha$ with t_{NM1} follows

$$\alpha_{\text{sp}} = \alpha_{\text{sp}}^\infty \frac{4 + \sqrt{3/\epsilon}}{4 + \sqrt{3/\epsilon}\,\frac{4 + \tanh\left(t_{\text{NM1}}/\lambda_{\text{sf}}\right) r\sqrt{3/\epsilon}}{4\tanh\left(t_{\text{NM1}}/\lambda_{\text{sf}}\right) + r\sqrt{3/\epsilon}}}, \tag{8}$$

where r is the ratio of $g_{\text{NM1/NM2}}^{\uparrow\downarrow}/g_{\text{FM/NM1}}^{\uparrow\downarrow}$. With $r = 0$ the two systems are decoupled, giving the same result as Eq. (5).

Films were fabricated from a base pressure of 10^{-8} Torr using magnetron sputtering with a working pressure of 10^{-3} Torr of Ar onto thermally oxidized Si wafers. For Pt NM layers, a series of samples with varying Pt thickness (0–2 nm) were grown in both NM/FM and FM/NM layer configurations, where the FM layer was Co or CoFeB. For each Pt thickness the FM thickness was varied to determine $g_{\text{eff}}^{\uparrow\downarrow}$. For Co, the thickness was varied from 2 to 5 nm to maintain an fcc structure that forms during the early stage growth structure, and for amorphous CoFeB from 2 to 15 nm. For both of these FM layers, the linear dependence of $4\pi\,\Delta\alpha/\gamma$ against $1/t_{\text{FM}}$ indicates there was no change in structure of the FM layer [55], as previously noted for Co [27]. All Pt samples were capped with a protective 2-nm layer of Ta, which formed an oxide layer that has negligible contributions to the spin pumping, as reported elsewhere [16]. For Ru layers, the thickness was varied up to 9 nm. Ru has hcp texture, and as such only NM capped FM layers were grown, to prevent the hcp texture influencing the fcc growth of sub-5-nm Co. The fcc Co samples were obtained below 5 nm and hcp Co between 10 and 30 nm. The Ru samples were capped with 5 nm of Cu.

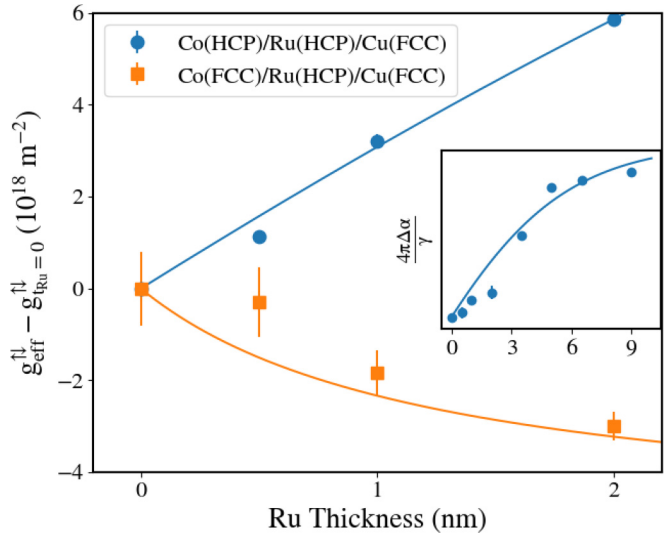

FIG. 2. The variation in $g_{\text{eff}}^{\uparrow\downarrow}$ for Co/Ru interfaces as a function of Ru thickness with either hcp or fcc Co. The graphs are scaled by subtracting $g_{\text{eff}}^{\uparrow\downarrow}$ with no Ru, which is 4.8×10^{18} m^{-2} for fcc and 0.1×10^{18} m^{-2} for hcp. The inset shows the evolution of the measured linewidth for the hcp Co case, over the full range of Ru thickness studied. The data are fitted to Eq. (8), with a spin-diffusion length from Eq. (7).

III. RESULTS AND DISCUSSION

Analysis of the damping from Pt and Ru interfaced layers involved fitting $\Delta\alpha/\gamma$ and $g_{\uparrow\downarrow}^{\text{eff}}$ as a function of NM thickness for each fixed FM thickness simultaneously, to extract the best fitting values for λ_{sf} and ϵ (see Fig. 2 for Co/Ru and Fig. 3 for Co/Pt, Pt/Co, CoFeB/Pt, and Pt/CoFeB). The best fitting interfacial transport parameters are summarized in Table I.

For the Co/Ru/Cu system, $g_{\text{eff}}^{\uparrow\downarrow}$ increases for Co(hcp)/Ru(hcp) structures with increasing Ru thickness

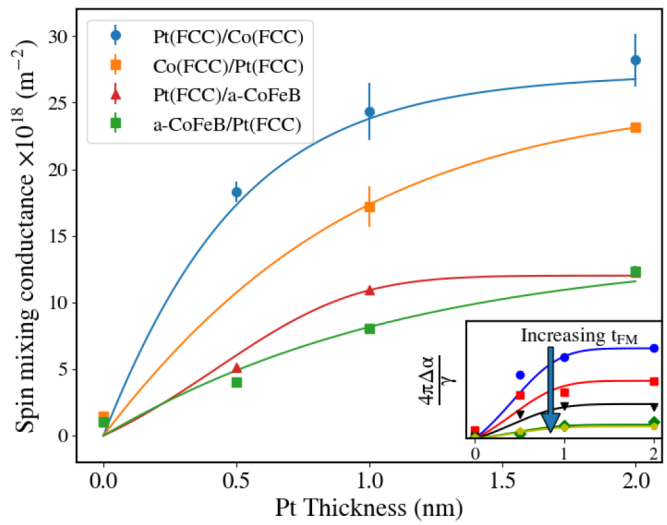

FIG. 3. The evolution of $g_{\text{eff}}^{\uparrow\downarrow}$ with Pt thickness for fcc Co, and amorphous CoFeB, with Pt on different interfaces. The inset is $\Delta 4\pi\alpha/\gamma$ for Pt/CoFeB samples with increasing FM thickness from top to bottom. Data fitted to Eq. (6), with the inset fitted to Eq. (5). In both cases the spin-diffusion length was fitted to Eq. (7).

TABLE I. Interfacial spin-transport parameters extracted from fitting the thickness dependence of both the NM and FM layers.

Sample	Spin-flip probability ϵ	Spin-diffusion length		$g_{\infty}^{\uparrow\downarrow}$ ($\times 10^{18}$)	r
		Constant λ_{sf}	Thickness-dependent λ_{∞}		
Co(hcp)/Ru(hcp)/Cu	$3.8 \pm 0.4 \times 10^{-3}$	7.0 ± 0.5 nm	22 ± 1 nm	16 ± 4 m^{-2}	$5.6 \pm 0.2 \times 10^{-4}$
Co(fcc)/Ru(hcp)/Cu	$3.1 \pm 0.6 \times 10^{-3}$	7.0 ± 0.5 nm	22 ± 1 nm	0.6 ± 0.4 m^{-2}	$1.4 \pm 0.8 \times 10^{1}$
Pt(fcc)/Co(fcc)	$1.7 \pm 0.4 \times 10^{-1}$	1.6 ± 0.6 nm	9.4 ± 0.7 nm	90 ± 10 m^{-2}	
Co(fcc)/Pt(fcc)	$2.6 \pm 0.7 \times 10^{-1}$	1.6 ± 0.6 nm	9.5 ± 0.6 nm	75 ± 6 m^{-2}	
Pt(fcc)/*a*-CoFeB	$1.1 \pm 0.5 \times 10^{-1}$	1.6 ± 0.6 nm	6.6 ± 0.8 nm	47 ± 5 m^{-2}	
a-CoFeB/Pt(fcc)	$1.0 \pm 0.3 \times 10^{-1}$	1.6 ± 0.6 nm	6.8 ± 0.7 nm	54 ± 7 m^{-2}	

relative to Co/Cu. This may be attributed to the matching of crystal structures at the interface compared to Co(hcp)/Cu(fcc). Also, as the Ru thickness increases further, $\Delta\alpha$ and $g_{\text{eff}}^{\uparrow\downarrow}$ tend to saturation as the thickness approaches the spin-diffusion length, as shown in the inset in Fig. 2. For the Co(fcc)/Ru(hcp) case, the introduction of Ru results in a decrease of the effective spin-mixing conductance compared to Co(fcc)/Cu(fcc), indicating a more opaque interface to spin propagation. A similar reduction of damping with an hcp material between two fcc layers was observed by Yakata *et al.* [19] for NiFe/Ru/Pt. The FM/NM1/NM2 system allows Eq. (8) to be used. Whereas previous studies attributed the decrease in interfacial damping to a change of the NM1/NM2 spin mixing (changing the r parameter), here, the reduction is due to a difference in structure across the FM/NM1 interface. For the Co(hcp)/Ru(hcp)/Cu(fcc) case, r is reduced such that the system behaves as if it were effectively FM/NM1 only, while for the Co(fcc)/Ru(hcp)/Cu(fcc) case, r increases with t_{Ru} thickness such that $g_{\text{eff}}^{\uparrow\downarrow}$ falls. Yakata *et al.* also observed a slight increase in damping for a NiFe(fcc)/Ru(hcp) system with a larger Ru thickness, but the increase was much smaller than Co(hcp)/Ru(hcp). ϵ for both Ru cases is much lower than for Pt, and λ_{sf} is more than twice that of Pt, as expected [8].

The evolution of both $g_{\text{eff}}^{\uparrow\downarrow}$ and $\Delta 4\pi\alpha/\gamma$ as a function of Pt thickness is shown in Fig. 3 for Co(fcc) and amorphous CoFeB. An interfacial difference is observed in $g_{\text{eff}}^{\uparrow\downarrow}$ with Co(fcc)/Pt(fcc) and Pt(fcc)/Co(fcc), that is attributed to a subtle difference in local structure. Interface-structure-dependent behavior in the Co/Pt system was also observed for the proximity-induced moment in Pt [58], with a twofold difference in total moment between the interfaces.

With an amorphous FM layer, as shown in Fig. 3, there is a significant reduction in $g_{\text{eff}}^{\uparrow\downarrow}$ compared to interfacing with a crystalline Co layer, for the same NM thickness. The final value reached is also independent of the interface, within error, however, before a complete layer of Pt is formed, there is a higher spin-mixing conductance for the bottom interface. Structural studies of Pt on amorphous CoFeTaB layers showed a change in the texture of sub-2-nm Pt layers [59].

The effect of including a thickness-dependent λ_{sf} in the analysis is shown in Table I. Fitting with a constant λ_{sf} gives values typical of previous FMR analyses between 1 and 2 nm [13,18], but here, the inclusion of a NM layer thickness dependence gives bulk λ_{sf} close to 10 nm, as reported elsewhere [24,29,60]; this resolves the discrepancy between values of λ_{sf} from different methods. The magnitude of ϵ for Pt supports reports that the EY mechanism is the dominant source of spin-flip scattering [41] and is of a similar order of magnitude (10^{-1}) to reported values [2].

IV. CONCLUSIONS

In conclusion, a detailed exploration of both FM and NM layers provides deeper insight into spin transport across interfaces in spintronic systems. Regardless of the interface, the transport properties of Ru and Pt layers are governed by the EY mechanism. For Ru, a lower spin-flip scattering probability compared to Pt with a longer spin-diffusion length, while most significantly the inclusion of a thickness-dependent spin-diffusion length resolves the discrepancies in the reported values of the spin-diffusion length for Pt.

Data presented within this article can be found at [61].

ACKNOWLEDGMENTS

Funding is acknowledged from EPSRC for the studentship for C.S., 1771248, Ref. No. EP/P510476/1.

[1] J. E. Hirsch, Phys. Rev. Lett. **83**, 1834 (1999).
[2] Y. Tserkovnyak, A. Brataas, and G. E. W. Bauer, Phys. Rev. Lett. **88**, 117601 (2002).
[3] O. R. Sulymenko, O. V. Prokopenko, V. S. Tiberkevich, A. N. Slavin, B. A. Ivanov, and R. S. Khymyn, Phys. Rev. Appl. **8**, 064007 (2017).
[4] M. Weiler, M. Althammer, M. Schreier, J. Lotze, M. Pernpeintner, S. Meyer, H. Huebl, R. Gross, A. Kamra, J. Xiao, Y.-T. Chen, H. J. Jiao, G. E. W. Bauer, and S. T. B. Goennenwein, Phys. Rev. Lett. **111**, 176601 (2013).
[5] H. Kurt, R. Loloee, K. Eid, W. P. Pratt, and J. Bass, Appl. Phys. Lett. **81**, 4787 (2003).
[6] J. C. Rojas-Sánchez, N. Reyren, P. Laczkowski, W. Savero, J. P. Attané, C. Deranlot, M. Jamet, J. M. George, L. Vila, and H. Jaffrès, Phys. Rev. Lett. **112**, 106602 (2014).
[7] V. P. Amin and M. D. Stiles, Phys. Rev. B **94**, 104419 (2016).
[8] Y. Tserkovnyak, A. Brataas, and G. E. W. Bauer, Phys. Rev. B **66**, 224403 (2002).
[9] M. A. Khasawneh, C. Klose, W. P. Pratt, and N. O. Birge, Phys. Rev. B **84**, 014425 (2011).

[10] D. Bozec, M. A. Howson, B. J. Hickey, S. Shatz, N. Wiser, E. Y. Tsymbal, and D. G. Pettifor, Phys. Rev. Lett. **85**, 1314 (2000).

[11] C. Stamm, C. Murer, M. Berritta, J. Feng, M. Gabureac, P. M. Oppeneer, and P. Gambardella, Phys. Rev. Lett. **119**, 087203 (2017).

[12] W. Zhang, W. Han, X. Jiang, S. H. Yang, and S. S. Parkin, Nat. Phys. **11**, 496 (2015).

[13] W. Zhang, V. Vlaminck, J. E. Pearson, R. Divan, S. D. Bader, and A. Hoffmann, Appl. Phys. Lett. **103**, 242414 (2013).

[14] D. Wei, M. Obstbaum, M. Ribow, C. H. Back, and G. Woltersdorf, Nat. Commun. **5**, 3768 (2014).

[15] M. Caminale, A. Ghosh, S. Auffret, U. Ebels, K. Ollefs, F. Wilhelm, A. Rogalev, and W. E. Bailey, Phys. Rev. B **94**, 014414 (2016).

[16] E. Montoya, P. Omelchenko, C. Coutts, N. R. Lee-Hone, R. Hübner, D. Broun, B. Heinrich, and E. Girt, Phys. Rev. B **94**, 054416 (2016).

[17] A. Ruiz-Calaforra, T. Brächer, V. Lauer, P. Pirro, B. Heinz, M. Geilen, A. V. Chumak, A. Conca, B. Leven, and B. Hillebrands, J. Appl. Phys. **117**, 163901 (2015).

[18] M. Belmeguenai, M. S. Gabor, F. Zighem, N. Challab, T. Petrisor, R. B. Mos, and C. Tiusan, J. Phys. D: Appl. Phys. **51**, 045002 (2018).

[19] S. Yakata, Y. Ando, T. Miyazaki, and S. Mizukami, Jpn. J. Appl. Phys **45**, 3892 (2006).

[20] A. Ghosh, S. Auffret, U. Ebels, and W. E. Bailey, Phys. Rev. Lett. **109**, 127202 (2012).

[21] K. Kondou, H. Sukegawa, S. Mitani, K. Tsukagoshi, and S. Kasai, Appl. Phys. Express **5**, 73002 (2012).

[22] J. C. Sánchez, L. Vila, G. Desfonds, S. Gambarelli, J. P. Attané, J. M. De Teresa, C. Magén, and A. Fert, Nat. Commun. **4**, 2944 (2013).

[23] A. J. Berger, E. R. J. Edwards, H. T. Nembach, O. Karis, M. Weiler, and T. J. Silva, Phys. Rev. B **98**, 024402 (2018).

[24] Y. Niimi, D. Wei, H. Idzuchi, T. Wakamura, T. Kato, and Y. C. Otani, Phys. Rev. Lett. **110**, 016805 (2013).

[25] M. Morota, Y. Niimi, K. Ohnishi, D. H. Wei, T. Tanaka, H. Kontani, T. Kimura, and Y. Otani, Phys. Rev. B **83**, 174405 (2011).

[26] E. Barati, M. Cinal, D. M. Edwards, and A. Umerski, Phys. Rev. B **90**, 014420 (2014).

[27] M. Tokaç, S. A. Bunyaev, G. N. Kakazei, D. S. Schmool, D. Atkinson, and A. T. Hindmarch, Phys. Rev. Lett. **115**, 056601 (2015).

[28] A. B. Cahaya, A. O. Leon, and G. E. W. Bauer, Phys. Rev. B **96**, 144434 (2017).

[29] O. Mosendz, J. E. Pearson, F. Y. Fradin, G. E. W. Bauer, S. D. Bader, and A. Hoffmann, Phys. Rev. Lett. **104**, 046601 (2010).

[30] S. Azzawi, A. Ganguly, M. Tokaç, R. M. Rowan-Robinson, J. Sinha, A. T. Hindmarch, A. Barman, and D. Atkinson, Phys. Rev. B **93**, 054402 (2016).

[31] A. Conca, B. Heinz, M. R. Schweizer, S. Keller, E. T. Papaioannou, and B. Hillebrands, Phys. Rev. B **95**, 174426 (2017).

[32] N. Behera, M. S. Singh, S. Chaudhary, D. K. Pandya, P. K. Muduli, N. Behera, M. S. Singh, S. Chaudhary, D. K. Pandya, and P. K. Muduli, J. Appl. Phys. **117**, 17A714 (2015).

[33] A. G. Kolesnikov, M. E. Stebliy, A. V. Ognev, A. S. Samardak, A. N. Fedorets, V. S. Plotnikov, X. Han, and L. A. Chebotkevich, J. Phys. D: Appl. Phys. **49**, 425302 (2016).

[34] J. Miyawaki, D. Matsumura, H. Abe, T. Ohtsuki, E. Sakai, K. Amemiya, and T. Ohta, Phys. Rev. B **80**, 020408 (2009).

[35] X. Qiu, W. Legrand, P. He, Y. Wu, J. Yu, R. Ramaswamy, A. Manchon, and H. Yang, Phys. Rev. Lett. **117**, 217206 (2016).

[36] R. J. Elliott, Phys. Rev. **96**, 266 (1954).

[37] Y. Yafet, Solid State Phys. **14**, 1 (1963).

[38] L. Szolnoki, B. Dóra, A. Kiss, J. Fabian, and F. Simon, Phys. Rev. B **96**, 245123 (2017).

[39] M. I. D'yakonov and V. I. Perel, Sov. Phys. Solid State **13**, 3023 (1972).

[40] E. Sagasta, Y. Omori, M. Isasa, M. Gradhand, L. E. Hueso, Y. Niimi, Y. C. Otani, and F. Casanova, Phys. Rev. B **94**, 060412(R) (2016).

[41] M.-H. Nguyen, D. C. Ralph, and R. A. Buhrman, Phys. Rev. Lett. **116**, 126601 (2016).

[42] S. Azzawi, A. T. Hindmarch, and D. Atkinson, J. Phys. D: Appl. Phys. **50**, 473001 (2017).

[43] I. Barsukov, F. M. Römer, R. Meckenstock, K. Lenz, J. Lindner, S. Hemken to Krax, A. Banholzer, M. Körner, J. Grebing, J. Fassbender, and M. Farle, Phys. Rev. B **84**, 140410(R) (2011).

[44] K. Baberschke, J. Phys.: Conf. Ser. **324**, 012011 (2011).

[45] C. Kittel, Phys. Rev. **73**, 155 (1948).

[46] J. Pelzl, R. Meckenstock, D. Spoddig, F. Schreiber, J. Pflaum, and Z. Frait, J. Phys.: Condens. Matter **15**, S451 (2003).

[47] A. N. Anisimov, M. Farle, P. Poulopoulos, W. Platow, K. Baberschke, P. Isberg, R. Wäppling, A. M. N. Niklasson, and O. Eriksson, Phys. Rev. Lett. **82**, 2390 (1999).

[48] L. Chen, S. Mankovsky, S. Wimmer, M. A. Schoen, H. S. Körner, M. Kronseder, D. Schuh, D. Bougeard, H. Ebert, D. Weiss, and C. H. Back, Nat. Phys. **14**, 490 (2018).

[49] J. P. Nibarger, R. Lopusnik, Z. Celinski, and T. J. Silva, Appl. Phys. Lett. **83**, 93 (2003).

[50] R. M. Rowan-Robinson, A. T. Hindmarch, and D. Atkinson, Phys. Rev. B **90**, 104401 (2014).

[51] K. Fuchs, Math. Proc. Cambridge Philos. Soc. **34**, 100 (1938).

[52] E. H. Sondheimer, Adv. Phys. **1**, 1 (1952).

[53] A. F. Mayadas and M. Shatzkes, Phys. Rev. B **1**, 1382 (1970).

[54] D. Alcer and D. Atkinson, Nanotechnology **28**, 375703 (2017).

[55] See Supplemental Material at http://link.aps.org/supplemental/10.1103/PhysRevB.99.064406 for a further description, which includes Refs. [56,57].

[56] Y.-T. Chen, S. Takahashi, H. Nakayama, M. Althammer, S. T. B. Goennenwein, E. Saitoh, and G. E. W. Bauer, Phys. Rev. B **87**, 144411 (2013).

[57] X.-G. Wang, Z.-W. Zhou, Y.-Z. Nie, Q.-L. Xia, and G.-H. Guo, Phys. Rev. B **97**, 094401 (2018).

[58] R. M. Rowan-Robinson, A. A. Stashkevich, Y. Roussigné, M. Belmeguenai, S. M. Chérif, A. Thiaville, T. P. Hase, A. T. Hindmarch, and D. Atkinson, Sci. Rep. **7**, 16835 (2017).

[59] O.-O. Inyang, Magnetic proximity effect and interfacial spin dependent transport in ferromagnet/heavy metal thin films, Ph.D. thesis, Durham University, 2018.

[60] H. Y. T. Nguyen, W. P. Pratt, and J. Bass, J. Magn. Magn. Mater. **361**, 30 (2014).

[61] C. Swindells, A. T. Hindmarch, A. J. Gallant, and D. Atkinson, Spin transport across the interface in ferromagnetic/nonmagnetic systems, https://doi.org/10.15128/r27m01bk728 (2019).